Weierstraß-Institut
für Angewandte Analysis und Stochastik

Leibniz-Institut im Forschungsverbund Berlin e. V.

Preprint ISSN 2198-5855

Cardiac dynamics of a human ventricular tissue model with focus on early afterdepolarizations

André H. Erhardt

submitted: December 2, 2024

Weierstrass Institute
Mohrenstr. 39
10117 Berlin
Germany
E-Mail: andre.erhardt@wias-berlin.de

No. 3147
Berlin 2024

2020 *Mathematics Subject Classification.* 92B25, 92C05, 37G15,37M05, 37N25.

Key words and phrases. Cardiac dynamics, bifurcations analysis, early afterdepolarization, monodomain equation, pattern formation.

The author acknowledges the funding by the German Research Foundation (DFG) within the DFG Priority Program SPP 2171 *Dynamic Wetting of Flexible, Adaptive, and Switchable Substrates* through the project 422786086.

Edited by
Weierstraß-Institut für Angewandte Analysis und Stochastik (WIAS)
Leibniz-Institut im Forschungsverbund Berlin e. V.
Mohrenstraße 39
10117 Berlin
Germany

Fax: +49 30 20372-303
E-Mail: preprint@wias-berlin.de
World Wide Web: http://www.wias-berlin.de/

Cardiac dynamics of a human ventricular tissue model with focus on early afterdepolarizations

André H. Erhardt

Abstract

The paper is aimed to investigate computationally complex cardiac dynamics of the famous human ventricular model of ten Tusscher and Panfilov from 2006. The corresponding physical system is modeled by a set of nonlinear differential equations containing various of system parameters. In case a specific physical parameter crosses a certain threshold, the system is forced to change dynamics, which might result in dangerous cardiac dynamics and can be precursors to cardiac death. For the performance of an efficient numerical analysis the original model is remodeled and simplified in such a way that the modified models perfectly matches the trajectory of the original model. Moreover, it is demonstrated that the simplified models have the same dynamics. Furthermore, using the lowest dimensional model it is systematically shown by means of bifurcation analysis that combinations of reduced slow and rapid potassium channels and enhanced sodium channel may lead to early afterdepolarizations. Finally, synchronization and the effect of EADs on larger scale (macro scale) is investigated numerically by studying the corresponding monodomain model. To this end we study the pattern formation of an one dimensional network of epi-, mid-myo- and endocardial cells and a two dimensional epicardial monodomain equation.

1 Introduction

Computational physiology and medicine, mathematics for healthcare and modeling of biomedical applications have gained importance in numerous interdisciplinary and multidisciplinary research projects in recent years, see for instance [1, 2, 3, 4]. Mathematical modeling has become an integral part and contributes significantly to a better understanding of real-world phenomena, such as cardiac or neuronal dynamics [5, 6, 7, 8, 9, 10, 11, 12, 13, 14]. In addition to mathematical modeling and simulations, the analysis of these complex systems is increasingly becoming the focus of research. Furthermore, in the field of mathematical and computational cardiology a strong focus is on the investigation of certain cardiac arrhythmia such as early afterdepolarizations (EADs). EADs are pathological voltage oscillations during the repolarization or plateau phase of cardiac action potentials (APs), cf. Figure 1, and are considered as potential precursors of cardiac arrhythmia, often associated with potassium deficiency or elevated calcium or sodium currents, e.g. caused by ion channel diseases, drugs or oxidative stress.

Very powerful tools to systematically analyze the dynamics of cardiac myocytes are bifurcation theory [15] and geometric singular perturbation theory [16], please see for instance recent studies in [17, 18, 19, 20, 21, 22, 23, 24, 25, 26, 27, 28, 29] and the references contained therein. These computational studies can be used to develop new therapies and help in improving clinical decision [30, 31, 32, 33, 34].

Bifurcation theory. In general, a state of a physical system can be observed when it is stable and one expects that a small change in a system parameter should not change the dynamics of the system. Rather, stable solutions can be expected to continuously change in unique ways. No dramatic change is observed when varying any parameter as long as a continuous solution branch retains its stability. However, when a certain physical parameter exceeds a threshold, the physical system may be forced to change its dynamics and complex behavior may result. Therefore, bifurcation theory is used to explain certain phenomena and dynamics of the famous TP06 model. One requirement to be able

DOI 10.20347/WIAS.PREPRINT.3147 Berlin 2024

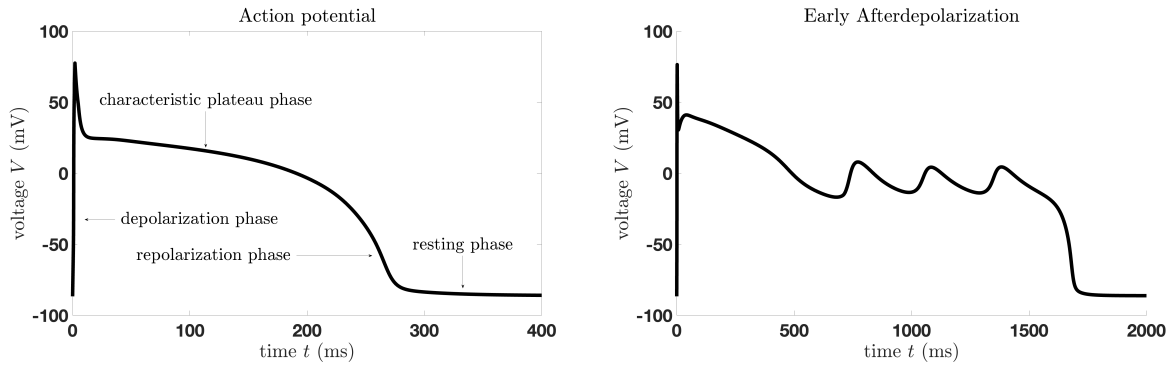

Figure 1: Simulations of TP06 human ventricular cell model. (**Left**) A characteristic action potential. (**Right**) An early afterdepolarizations.

to apply bifurcation theory is that the investigated system is sufficiently smooth. However, this is not the case for the original TP06 model, which is independently reported in [35, 36]. In [35], the authors modified the sodium current I_{Na} similar to the approach used in [37], while in [36] the sodium current I_{Na} was modified using the idea from [38]. Both approaches enable to perform (numerical) bifurcation analysis with slight differences. The advantage of the approach used in [35] is that the remodeled system almost always perfectly fits the original TP06 model without changing the stimulus, while the ansatz in [36] leads to a almost perfect remodeling of the original TP06 model. On the other hand the ansatz in [36] results in a lower dimensional model and therefore, the bifurcation analysis is more efficient. These advantages and disadvantages one has to take into account.

Numerical methods. For our simulations we utilize MATLAB R2023b and Python 3.9 with FEniCS [39, 40]. For solving the ODE system we mainly use the MATLAB ode solver *ode15s* with a relative tolerance of 10^{-13} and an absolute tolerance of 10^{-18}. For the monodomain model, the *pdepe* solver is used for the one dimensional case and the two dimensional simulations are done in FEniCS [39, 40], where the coupled ODE–PDE system is solved using cbcbeat [41], and fenics-beat [42]. We want to highlight that cbcbeat and fenics-beat use a second order splitting scheme with Crank-Nicolson method for the time stepping. Moreover, the Rush and Larsen scheme [43] is used to integrate the gating variables in time. For the bifurcation analysis we use `CL_MATCONT`, *a continuation toolbox for MATLAB* [44, 45]. The codes are available via [46].

Aim and motivation of the paper. The aim of this paper is the analysis of cardiac dynamics, where the corresponding physical system is modeled by a set of nonlinear differential equations. This is motivated by the following: Cardiac myocytes can exhibit complex oscillatory patterns such as spiking and bursting that are related to ion current interactions. In addition to normal APs of a cardiac myocyte, certain types of cardiac arrhythmias can occur. These include certain types of cardiac arrhythmias that can lead to sudden cardiac death. Furthermore, irregular behavior such as (deterministic) chaos or chaotic EADs has been observed in both experimental and computational studies, cf. [47, 48, 49, 50] and the references contained therein. Moreover, the heart dynamics or heart rhythm can react very sensitively to the influence of certain medications and computational studies can give new insights and can help to make better predictions, cf. [51, 52, 53, 54, 55]. To this end, we modified and simplified the cardiac muscle cell model by ten Tusscher and Panfilov from 2006 (TP06 model, [56, 57]) to perform numerical bifurcation analysis. This allows to investigate the dynamics of the TP06 model and to predict the occurrence of normal APs or cardiac arrhythmia such as EADs. The focus of this study is on the model reduction and enhancement of the efficiency of the numerical bifurcation analysis without loss of information to the original TP06 model.

Our modifications presented in this paper reduce the complexity of the 19 dimensional TP06 model in several steps to a 18 dimensional, 16 dimensional and 14 dimensional system with astonishing consistency with the original model, please see Figure 2 and Figure 3. Here, we changed the conductance of the slow delayed rectifier current $\mathrm{I_{Ks}}$, rapid delayed rectifier current $\mathrm{I_{Kr}}$ and the sodium current $\mathrm{I_{Na}}$ such that $(\mathrm{G_{Ks}}, \mathrm{G_{Kr}}, \mathrm{G_{CaL}}) \longrightarrow (\mathrm{G_{Ks}}, 0.18 \cdot \mathrm{G_{Kr}}, 5 \cdot \mathrm{G_{CaL}})$. Beside the modifications and model

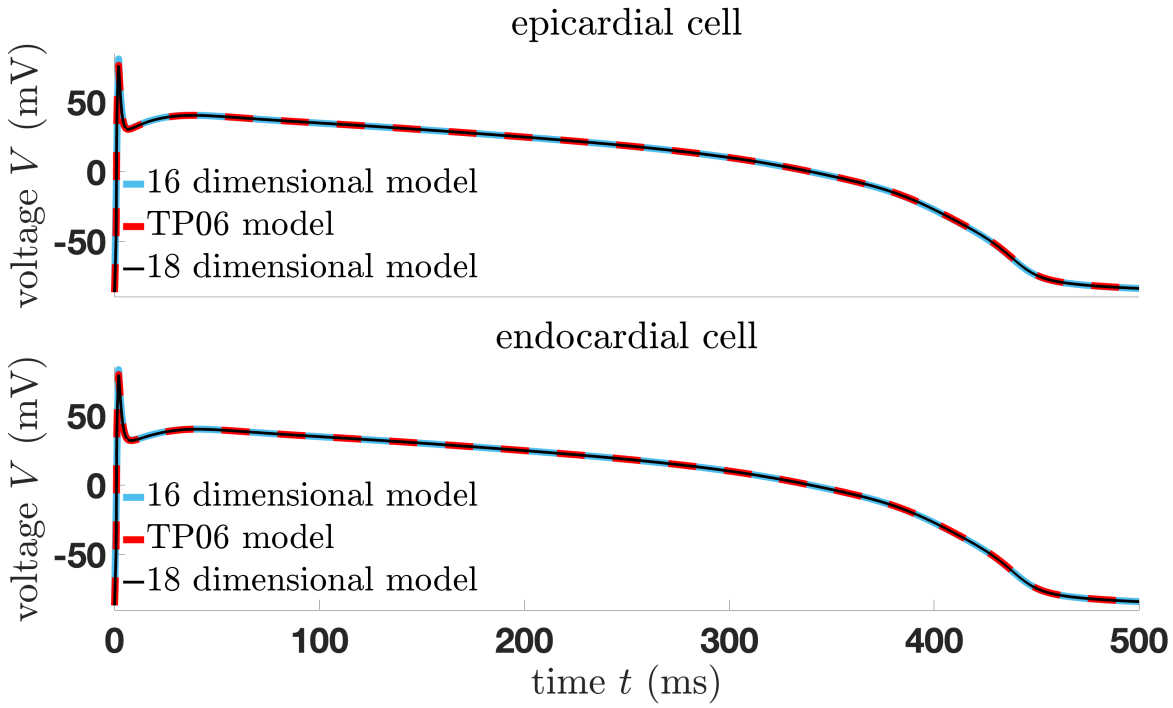

Figure 2: Comparison of the modified models and original TP06 human ventricular epi- and endocardial cell model.

reduction which we will present in the next section, we have to adjust the initial stimulus for the 16 dimensional model in Figure 2, i.e. we used $\mathrm{I_{stim}} = 89\frac{pA}{pF}$ instead of $\mathrm{I_{stim}} = 52\frac{pA}{pF}$. Moreover, the effect of the different stimuli one can nicely observe in Figure 3. In the first row of Figure 3 an initial stimulus of $\mathrm{I_{stim}} = 52\frac{pA}{pF}$ is applied to the 16 dimensional model. Although the trajectories do not match perfectly the dynamics are similar. In the second row of Figure 3 perfectly matching trajectories of the TP06 model and its different versions are shown highlighting if a different stimulus is applied. Notice that the MATLAB code to produce Figure 2 and Figure 3 is provided in [46]. Using this code, the readers can also convince themselves that the modified systems approximate the original system very well.

Plan of the paper. In this paper, we will first modify and simplify the TP06 model and then, we compare the dynamics of the resulting three modified TP06 models – one 18 dimensional, one 16 dimensional and one 14 dimensional system of ordinary differential equations (ODEs). The 18 dimensional model is in the fashion of [37, 35] and perfectly represents the original model, while the 16 dimensional model gives a perfect approximation of the original model in case we modify the initial stimulus. The same applies to the 14 dimensional model. Notice that without the modification of the initial stimulus the models show very similar dynamics compared to the original one, however, the trajectories do not perfectly coincide with the one from the TP06 model. Furthermore, we will analyze the new developed systems by means of bifurcation theory. Here, we will focus mainly on the 14 dimensional case. Finally, we will perform a numerical experiments of the corresponding heart model.

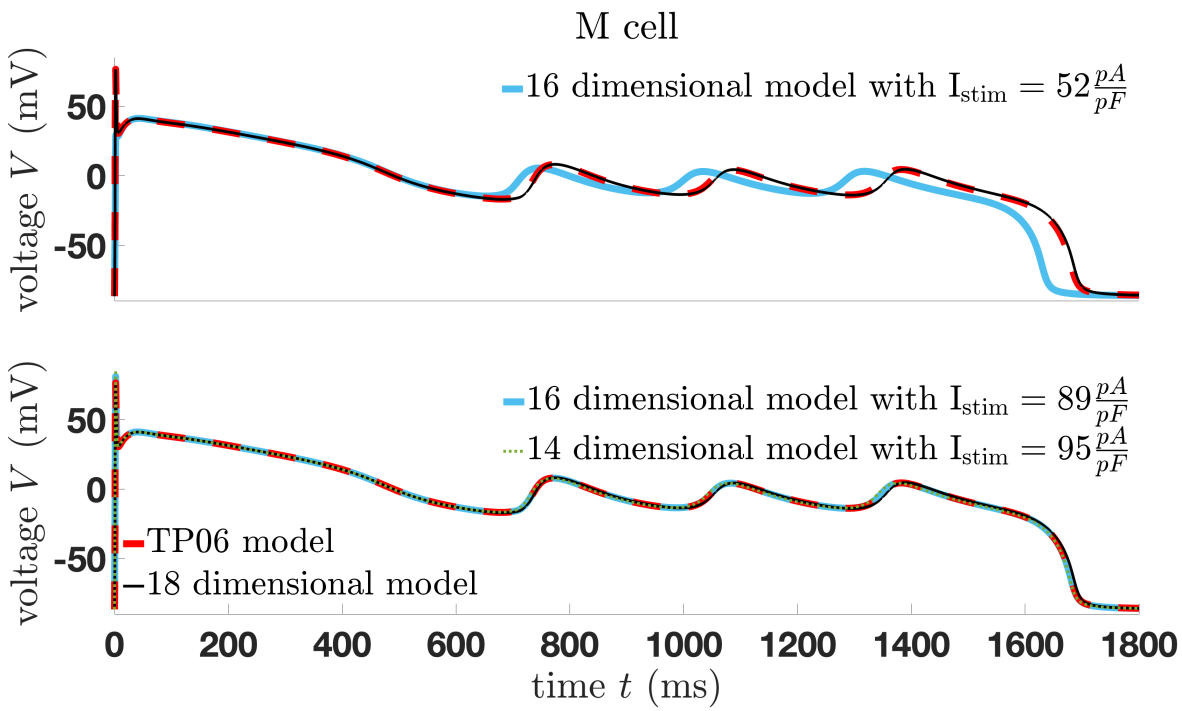

Figure 3: Comparison of the modified and original TP06 human ventricular mid-myocardial cell model.

2 Cardiac modeling

Here, we briefly describe the cardiac model we will investigate in this paper.

2.1 Cardiac single cell model

Mathematical modeling of action potentials (APs) of excitable biological cells such as cardiac myocyte has its origin in the Hodgkin-Huxley model [58]. Here, an approach was developed to model APs of excitable biological cells through a system of ordinary differential equations (ODEs). These conductance-based models represent a minimal biophysical interpretation of excitable biological cells in which current flow across the membrane is due to the charging of membrane capacitance and the movement of ions through ion channels that are selective for certain ion species. An initial stimulus activates the ion channels once a certain threshold potential is reached. Then these ion channels open and/or close, allowing an ion current to flow that changes the membrane potential. This electrophysiological behavior of a cardiac myocyte is represented by the following ODE:

$$C_m \frac{\mathrm{d}V}{\mathrm{d}t} = -\mathrm{I}_{\mathrm{ion}} + \mathrm{I}_{\mathrm{stim}}, \tag{1}$$

where V denotes the voltage (in mV) and t the time (in ms), while $\mathrm{I}_{\mathrm{ion}}$ is the sum of all transmembrane ionic currents. The (epi-, mid-myo- and endocardial) human ventricular TP06 model contains several different ion currents, ion pump, ion exchanger and background currents, i.e.

$$\mathrm{I}_{\mathrm{ion}} = \mathrm{I}_{\mathrm{K1}} + \mathrm{I}_{\mathrm{to}} + \mathrm{I}_{\mathrm{Kr}} + \mathrm{I}_{\mathrm{Ks}} + \mathrm{I}_{\mathrm{CaL}} + \mathrm{I}_{\mathrm{NaK}} + \mathrm{I}_{\mathrm{Na}} + \mathrm{I}_{\mathrm{bNa}} + \mathrm{I}_{\mathrm{NaCa}} + \mathrm{I}_{\mathrm{bCa}} + \mathrm{I}_{\mathrm{pK}} + \mathrm{I}_{\mathrm{pCa}}.$$

These currents are depending on individual ionic conductances $\mathrm{G}_{\text{current}}$ and Nernst potentials $\mathrm{E}_{\text{current}}$. Moreover, they may depend on gating variables, which are important for the activation and inactivation of the ion currents. The gating variables satisfy the differential equation

$$\frac{\mathrm{d}g}{\mathrm{d}t} = a_g(1-g) - b_g g = a_g - (a_g + b_g)g = \frac{g_\infty - g}{\tau_g}, \tag{2}$$

where g represents the gating variables, while $g_\infty := g_\infty(V) = a_g \cdot (a_g + b_g)^{-1}$ denotes the equilibrium of the gating variable g and $\tau_g := \tau_g(V) = (a_g + b_g)^{-1}$ its time scale. Furthermore, the ionic concentrations of the TP06 model from [56, 57] reads as follows:

$$\begin{aligned}
\frac{\mathrm{d}\bar{R}}{\mathrm{d}t} &= -k_2[Ca]_{ss}\bar{R} + k_4(1-\bar{R}),\\
\frac{\mathrm{d}[Ca]_i}{\mathrm{d}t} &= \mathsf{Ca}_{\text{ibufc}}\left((\mathrm{I}_{\text{leak}} - \mathrm{I}_{\text{up}})\frac{V_{sr}}{V_c} + \mathrm{I}_{\text{xfer}} - \frac{(\mathrm{I}_{\text{bCa}} + \mathrm{I}_{\text{pCa}} - 2\mathrm{I}_{\text{NaCa}})}{2V_cF}\right),\\
\frac{\mathrm{d}[Ca]_{sr}}{\mathrm{d}t} &= \mathsf{Ca}_{\text{srbufsr}}(\mathrm{I}_{\text{up}} - (\mathrm{I}_{\text{rel}} + \mathrm{I}_{\text{leak}})),\\
\frac{\mathrm{d}[Ca]_{ss}}{\mathrm{d}t} &= \mathsf{Ca}_{\text{ssbufss}}\left(-\frac{\mathrm{I}_{\text{CaL}}}{2V_{ss}F} + \mathrm{I}_{\text{rel}}\frac{V_{sr}}{V_{ss}} - \mathrm{I}_{\text{xfer}}\frac{V_c}{V_{ss}}\right),\\
\frac{\mathrm{d}[Na]_i}{\mathrm{d}t} &= -\frac{\mathrm{I}_{\text{Na}} + \mathrm{I}_{\text{bNa}} + 3\mathrm{I}_{\text{NaK}} + 3\mathrm{I}_{\text{NaCa}}}{V_cF},\\
\frac{\mathrm{d}[K]_i}{\mathrm{d}t} &= -\frac{\mathrm{I}_{\text{K1}} + \mathrm{I}_{\text{to}} + \mathrm{I}_{\text{Kr}} + \mathrm{I}_{\text{Ks}} - 2\mathrm{I}_{\text{NaK}} + \mathrm{I}_{\text{pK}} + \mathrm{I}_{\text{stim}}}{V_cF}.
\end{aligned}$$

Note that we do not specify the constants, but they are available in [56, 57] or in the provided code in [46]. Furthermore, the main ion currents except the sodium current are listed in Table 1.

List of main ion currents	
Ion current description	name & gating variables
$\mathrm{I}_{\text{CaL}} = \mathrm{G}_{\text{CaL}} d\, f\, f_2\, f_{\text{Cass}} \frac{4(V-15)F^2}{RT} \frac{0.25\text{Ca}_{\text{ss}}\exp(2(V-15)\frac{F}{RT}) - \text{Ca}_{\text{o}})}{\exp(2(V-15)\frac{F}{RT})-1}$	L-type calcium current: d, f, $f2$ and f_{Cass}
$\mathrm{I}_{\text{to}} = \mathrm{G}_{\text{to}} r\, s(V - \mathrm{E}_{\text{K}})$	transient outward current: r and s
$\mathrm{I}_{\text{Ks}} = \mathrm{G}_{\text{Ks}} x_s^2 (V - \mathrm{E}_{\text{Ks}})$	slow delayed rectifier current: x_s
$\mathrm{I}_{\text{Kr}} = \mathrm{G}_{\text{Kr}} x_{r_1}\, x_{r_2} (V - \mathrm{E}_{\text{K}})$	rapid delayed rectifier current: x_{r_1} and x_{r_2}
$\mathrm{I}_{\text{K1}} = \mathrm{G}_{\text{K1}} x_{K1_\infty} (V - \mathrm{E}_{\text{K}})$	inward rectifier current

Table 1: Main ion currents, where the gating variables satisfy the differential equation (2).

Finally, we would like to highlight the difference between the epi-, mid-myo- and endocardial human ventricular TP06 model. There are two parts of the model which differ for these three cell types:

1 The modeling of the gating variable s of the transient outward current I_{to} is different, i.e.

$$s_\infty = \begin{cases} \dfrac{1}{1+e^{\frac{V+20}{5}}} & \text{for epicardial and M cells,} \\ \dfrac{1}{1+e^{\frac{V+28}{5}}} & \text{for endocardial cells} \end{cases}$$

and

$$\tau_s = \begin{cases} 85e^{-\frac{(V+45)^2}{320}} + \dfrac{5}{1+e^{\frac{V-20}{5}}} + 3 & \text{for epicardial and M cells,} \\ 1000e^{-\frac{(V+67)^2}{1000}} + 8 & \text{for endocardial cells.} \end{cases}$$

2 The value of $\mathrm{G_{to}}$ and $\mathrm{G_{Ks}}$ differ, i.e.

$$\mathrm{G_{to}} = \begin{cases} 0.294\dfrac{nS}{pF} & \text{for epicardial and M cells,} \\ 0.073\dfrac{nS}{pF} & \text{for endocardial cells} \end{cases}$$

and

$$\mathrm{G_{Ks}} = \begin{cases} 0.392\dfrac{nS}{pF} & \text{for epi- and endocardial cells,} \\ 0.098\dfrac{nS}{pF} & \text{for M cells.} \end{cases}$$

For a full description of the variables involved, please see [56, 57].

This also implies that we only need one proper bifurcation analysis with respect to $\mathrm{G_{Ks}}$ for epicardial and M cells, since the models are different only in $\mathrm{G_{Ks}}$. Furthermore, we need an analysis for endocardial cells separately. Moreover, this is also an explanation why the trajectories in Figure 2 and Figure 3 are different. For the simulations in Figure 2 and Figure 3 we used the same setting as in [57] expect for the value $\mathrm{G_{Kr}}$, which we set to 18% of the original value and the value $\mathrm{G_{CaL}}$, which we have chosen 5 times bigger than the one in [57]. Therefore, the M cell enters a region, where EADs occur.

2.2 Model modification and reduction

First, we remove the ODE representing the intracellular ion concentration $[K]_i$ and set $[K]_i$ constant equal to the initial concentration $[K]_i$ of the TP06 model, $[K]_i = 138.3\ mM$. Referring to [59], it has been postulated that models for cardiac cells that account for changes in intracellular ion concentrations violate a conservation principle. As a result these systems never reach a steady state, i.e. a resting potential, which is required to be able to apply bifurcation theory.

18 dimensional model In addition as pointed out in [36], the first issue is in the modeling of the sodium current in [56, 57], i.e.

$$\mathrm{I_{Na}} = \mathrm{G_{Na}} m^3 hj(V - \mathrm{E_{Na}}),$$

where G_{Na} denotes the ionic conductance and E_{Na} the Nernst potential, while the different gating variables m, h and j satisfy the differential equation (2). To be more precise, the issue appears in the modeling of the gating variables h and j, since the voltage dependent functions a_h, b_h, a_j and b_j are not continuous, cf. [56]. In the fashion of [37, 35], we introduce a new function

$$u = \frac{1}{1 + e^{-5(V+40)}}$$

and remodel the rate constants $\alpha_h, \beta_h, \alpha_j$ and β_j as follows:

$$\begin{aligned}
\alpha_h &= (1-u)0.057e^{\frac{-(V+80)}{6.8}}, \\
\beta_h &= \frac{0.77}{0.13\left(1 + e^{\frac{-(V+10.66)}{11.1}}\right)}u + (1-u)\left(2.7e^{0.079V} + 3.1 \cdot 10^5 e^{0.3485V}\right), \\
\alpha_j &= (1-u)\left(-2.5428 \cdot 10^4 e^{0.2444V} - 6.948 \cdot 10^{-6} e^{-0.04391V}\right)\frac{V + 37.78}{1 + e^{0.311(V+79.23)}}, \\
\beta_j &= 0.6\frac{e^{0.057V}}{1 + e^{-0.1(V+32)}}u + (1-u)\frac{0.02424e^{-0.01052V}}{1 + e^{-0.1378(V+40.14)}}.
\end{aligned}$$

Now, the modified model is sufficiently smooth without any discontinuity. Therefore, bifurcation analysis is applicable and no further modification are needed to fit the original model. Notice that the function u is modeled in such a way that $u = 0.5$ for $V = -40\ mV$ to represent the switching modeled in [56] of $\alpha_h, \beta_h, \alpha_j$ and β_j at $V = -40\ mV$, while the factor '-5' might be improvable.

16 dimensional model A further way to avoid the issue with the discontinuity of the rate constants $\alpha_h, \beta_h, \alpha_j$ and β_j is to notice that the equilibrium of h and j are equal. In [36] the gating variables h and j are reformulated to one new gating variable v, and modify the sodium current to

$$\mathrm{I}_{\mathrm{Na}} = \mathrm{G}_{\mathrm{Na}} m^3 v^2 (V - \mathrm{E}_{\mathrm{Na}})$$

and a new time scale was introduced such that v satisfies (2) with

$$v_\infty = h_\infty = j_\infty = \frac{1}{\left(1 + e^{\frac{V+71.55}{7.43}}\right)^2}$$

and the time relaxation constant is given by

$$\tau_v = 0.25 + \frac{2.24 \cdot v_\infty}{(1 - \tanh(6.468 + 0.07V))},$$

which could probably be improved. However, we realized that instead of considering a 17 dimensional model it is more practical to set $v = v_\infty = h_\infty = j_\infty$ and to adjust the initial stimulus. This removes the discontinuity and in addition, we reduce the model by a further dimension.

14 dimensional model Finally, in this fashion and motivated by [60] we also fixed two further gating variables equal to their steady state solutions, i.e. we fixed the gating variable r of the transient outward current I_{to} and the gating variable x_{r_2} of rapid delayed rectifier current I_{Kr} such that

$$r = r_\infty = \frac{1}{1 + e^{\frac{-(V+20)}{6}}} \qquad \text{and} \qquad x_{r_2} = x_{r_{2\infty}} = \frac{1}{1 + e^{\frac{V+88}{24}}}.$$

This requires again a modification of the initial stimulus, which has to be higher compared to the 16 dimensional model. However, this simplified model shows a remarkable accurate approximation of the original model and additionally it is much less challenging to analyze, which we will highlight later in more details.

2.3 Monodomain model

For the modeling of the heart one usually uses either the monodomain model, the bidomain model or the EMI model, which includes explicitly the extracellular space (E), the cell membrane (M) and the intracellular space (I) [61, 62], see also the Kirchhoff-Nernst-Planck-EMI model [63, 64] in a electroneutral framework. On the other hand monodomain models have been shown to be a good approximation for wave propagation in cardiac tissue, cf. e.g. [65] and are well studied, see e.g. [66, 67]. In addition, the monodomain model is a special case of the bidomain model assuming equal anisotropy rates, while in [68] it was showing that the bidomain model can be derived from the EMI model. Therefore, there is a clear link between these models and dependent on the propose of the study one has three models of different complexity available.

Notice the bidomain model [69] takes into account the anisotropy of both, intra- and extracellular spaces, i.e.

$$\begin{aligned} \nabla \cdot (M_i \nabla V) + \nabla \cdot (M_i \nabla V_e) &= \chi \left(C_m \frac{\partial V}{\partial t} + \mathrm{I}_{\mathrm{ion}}(V, g) - \mathrm{I}_{\mathrm{stim}} \right), \\ \nabla \cdot (M_i \nabla V) + \nabla \cdot ((M_i + M_e) \nabla V_e) &= 0 \end{aligned} \tag{3}$$

equipped with Neumann boundary conditions, where the extracellular potential V_e is given in terms of V and the intracellular potential V_i, i.e. $V_e = V_i - V$. M_i and M_e denote the intra- and extracellular conductivity tensors, and χ is the membrane surface area per unit volume. While the monodomain model

$$\frac{\lambda}{1+\lambda} \nabla \cdot (M_i \nabla V) = \chi \left(C_m \frac{\partial V}{\partial t} + \mathrm{I}_{\mathrm{ion}}(V, g) - \mathrm{I}_{\mathrm{stim}} \right) \tag{4}$$

derives from model (3) by assuming equal anisotropy rates $M_e = \lambda M_i$, where λ is a scalar constant. In this study we will focus on the monodomain model due to the fact that the TP06 model is also modeled as a monodomain model, cf. [56, 57].

3 Bifurcation analysis of the cardiac single cell model

The aim of the paper is to make statements about the behavior of the trajectories and the dynamics of the TP06 system. To this end, we investigate the stability and bifurcations of the modified systems, cf. [15, 70, 47, 35]. Moreover, we provide the corresponding codes in [46].

A bifurcation of a dynamical system is a qualitative change in its dynamics caused by the change of parameters. Therefore, we study the modified TP06 model by means of (numerical) bifurcation analysis using `CL_MATCONT`, *a continuation toolbox for MATLAB* [44, 45]. We consider an autonomous system of ordinary differential equations where the right-hand side of this system depends on several state variables and parameters. Therefore, we consider the modified TP06 models, containing 18, 16 or 14 state variables, without initial stimulus for the bifurcation analysis and we will focus our study on

the effect of a deficit in the fast and slow potassium current $\mathrm{I_{Kr}}$ and $\mathrm{I_{Ks}}$, and an enhancement in the sodium current $\mathrm{I_{CaL}}$.

The starting point of the bifurcation analysis is to determine an equilibrium of the modified autonomous system. To this end, one solve the algebraic equations

$$
\begin{aligned}
0 &= \mathrm{I_{K1}} + \mathrm{I_{to}} + \mathrm{I_{Kr}} + \mathrm{I_{Ks}} + \mathrm{I_{CaL}} + \mathrm{I_{NaK}} + \mathrm{I_{Na}} + \mathrm{I_{bNa}} + \mathrm{I_{NaCa}} + \mathrm{I_{bCa}} + \mathrm{I_{pK}} + \mathrm{I_{pCa}},\\
0 &= -k_2[Ca]_{ss}\bar{R} + k_4(1-\bar{R}),\\
0 &= \mathrm{Ca_{ibufc}}\left((\mathrm{I_{leak}} - \mathrm{I_{up}})\frac{V_{sr}}{V_c} + \mathrm{I_{xfer}} - \frac{(\mathrm{I_{bCa}} + \mathrm{I_{pCa}} - 2\mathrm{I_{NaCa}})}{2V_cF}\right),\\
0 &= \mathrm{Ca_{srbufsr}}(\mathrm{I_{up}} - (\mathrm{I_{rel}} + \mathrm{I_{leak}})),\\
0 &= \mathrm{Ca_{ssbufss}}\left(-\frac{\mathrm{I_{CaL}}}{2V_{ss}F} + \mathrm{I_{rel}}\frac{V_{sr}}{V_{ss}} - \mathrm{I_{xfer}}\frac{V_c}{V_{ss}}\right),\\
0 &= -\frac{\mathrm{I_{Na}} + \mathrm{I_{bNa}} + 3\mathrm{I_{NaK}} + 3\mathrm{I_{NaCa}}}{V_cF}
\end{aligned}
$$

with $g \equiv g_\infty(V)$, where g represents the gating variables. The next step is to derive the stability of the equilibrium determine the eigenvalues of the Jacobian or using the Routh-Hurwitz criterion, cf. [70, 47]. If we do so we are able to determine the stability of the modified systems dependent on the ionic conductances $\mathrm{G_{Ks}}$, $\mathrm{G_{Kr}}$ and $\mathrm{G_{CaL}}$ see Figure 4. Here, we have stable regions (black surfaces) and unstable regions (blue surfaces). In general, the unstable region allows the system to oscillate,

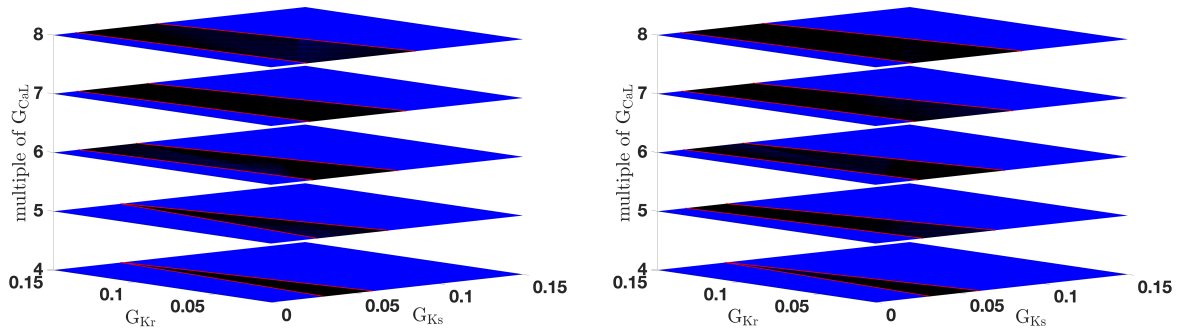

Figure 4: Multiple bifurcation analysis. Stable (black surface) and unstable (blue surface) region projected on the $(\mathrm{G_{Ks}}, \mathrm{G_{Kr}}, \mathrm{G_{CaL}})$-space. (**Left**) epicardial cell. (**Right**) endocardial cell.

i.e. after an initial stimulus the trajectory can either develop normal APs or other oscillatory behavior such as EADs or some sort of ventricular tachycardia for instance, which one cannot specify at this stage. However, in case the trajectory enters the stable region it will reach a stable equilibrium, which corresponds to the sudden death. Figure 4 also indicates that for increasing $\mathrm{G_{CaL}}$ and decreasing $\mathrm{G_{Ks}}$ and $\mathrm{G_{Kr}}$ the stable area becomes larger and the risk of a sudden death increases. This result is also compatible with the current state of knowledge. Moreover, Figure 4 shows also two red lines. These lines are the Andronov–Hopf bifurcation curves. At an Andronov–Hopf bifurcation the system changes stability via a pair of purely imaginary eigenvalues, i.e. $\lambda_{1,2} = \pm\mathbf{i}\omega_0$, $\omega_0 > 0$, and a limit cycle bifurcates.

Here, we want also to highlight that the standard value $\mathrm{G_{Kr}}$ is $0.153\frac{nS}{pF}$. Therefore, in case that $\mathrm{G_{CaL}}$ does not increase too much and $\mathrm{G_{Ks}}$ remains to its standard value, the risk that the cardiac myocte

TP06 model develops the sudden death is small, almost zero. However, if $\mathrm{G}_{\mathrm{CaL}}$ increases, e.g. by a factor 5 and G_{Kr} is small, the risk of a sudden death increases and the M cells already develop EADs for the standard value of G_{Ks} as we saw in Figure 3. Again, this is reasonable and compatible with the current state of knowledge, since it is known at EADs can be related to the limit cycle bifurcating from an Andronov–Hopf bifurcation, see e.g. [70, 47, 36], and from a medical point of view EADs can be precursors to the sudden cardiac death.

Our goal is to exam one parameter set $(\mathrm{G}_{\mathrm{Ks}}, \mathrm{G}_{\mathrm{Kr}}, \mathrm{G}_{\mathrm{CaL}})$ and to better understand the behavior of the (endocardial) cell model and to compare the stationary dynamics of the 18 dimensional, 16 dimensional and 14 dimensional model. A more practical way to analyze a dynamical system by means of bifurcation theory is to use the continuation algorithm from [44, 45]. Choosing the parameter set $(\mathrm{G}_{\mathrm{Ks}}, \mathrm{G}_{\mathrm{Kr}}, \mathrm{G}_{\mathrm{CaL}}) \longrightarrow (\mathrm{G}_{\mathrm{Ks}}, 0.1 \cdot \mathrm{G}_{\mathrm{Kr}}, 5 \cdot \mathrm{G}_{\mathrm{CaL}})$, and G_{Ks} as bifurcation parameter, we get two supercritical Andronov-Hopf bifurcations, cf. Table 2 and Table 3, which both generate a stable limit cycle and thus, the bifurcating limit cycles are both stable. Between these Andronov-Hopf bifurcations the system exhibits the stable equilibrium branch. Table 2 and Table 3 show that the three different models have almost identical Andronov-Hopf bifurcations.

	G_{Ks} value	Lyapunov exponent
18 dimensional	$0.027907858929580 \frac{nS}{pF}$	-2.683800872009436
16 dimensional	$0.027907858929578 \frac{nS}{pF}$	-2.683800872002161
14 dimensional	$0.027907284533354 \frac{nS}{pF}$	-2.667544014101886

Table 2: Comparison: First supercritical Andronov-Hopf bifurcation.

	G_{Ks} value	Lyapunov exponent
18 dimensional	$0.071030406847997 \frac{nS}{pF}$	$-1.961299057894090 \cdot 10^{-4}$
16 dimensional	$0.071030406847997 \frac{nS}{pF}$	$-1.961299057894896 \cdot 10^{-4}$
14 dimensional	$0.071026913636226 \frac{nS}{pF}$	$-1.964507593593568 \cdot 10^{-4}$

Table 3: Comparison: second supercritical Andronov-Hopf bifurcation.

Starting a limit cycle continuation from the second supercritical Andronov-Hopf bifurcation one derives a limit cycle branch containing a torus bifurcation and a (first) period-doubling bifurcation, cf. Table 4. Notice that this limit cycle branch is the reason for the occurrence of both AP and EADs, which we will highlight later more in detail.

	G_{Ks} value of the torus bifurcation	G_{Ks} value of the PD bifurcation
18 dimensional	$0.074450869484859 \frac{nS}{pF}$	$0.096093300233720 \frac{nS}{pF}$
16 dimensional	$0.074450869481487 \frac{nS}{pF}$	$0.096093300267257 \frac{nS}{pF}$
14 dimensional	$0.074412915016840 \frac{nS}{pF}$	$0.096081176095085 \frac{nS}{pF}$

Table 4: Comparison: torus bifurcation and period-doubling (PD) bifurcation of the first limit cycle branch.

It is remarkable that for the 18 dimensional, 16 dimensional and 14 dimensional not only the equilibrium curves are identical, which is obvious, but also the stability and the bifurcation points are identical up to a certain degree, which is visible in Tables 2, 3 and 4. This is also reflected in Figure 5, where one sees no differences. The first limit cycle branch (red surface) of the three simplified models is bifurcating from a supercritical Andronov–Hopf bifurcation (red dot). At the Andronov–Hopf bifurcation

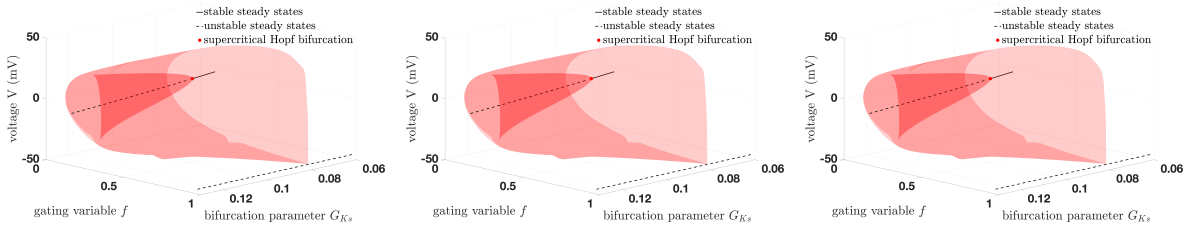

Figure 5: Comparison of the bifurcation diagrams using $\mathrm{G_{Ks}}$ as bifurcation parameter with value shifts $\mathrm{G_{Kr}} \to 0.1 \cdot \mathrm{G_{Kr}}$ and $\mathrm{G_{CaL}} \to 5 \cdot \mathrm{G_{CaL}}$. (**Left**) 18 dimensional model. (**Middle**) 16 dimensional model. (**Right**) 14 dimensional model.

the equilibrium curve (black line: the dashed part represents the unstable branch, the solid part the stable branch) also changes stability.

Here, we want to highlight that fixing more gating variables equal to its steady state solution will not change the equilibrium curve, however, it will change its stability and potential bifurcations points, and therefore, the dynamics of the whole system. Furthermore, in Figure 6 we see the limitation of the 18 dimensional model, since for the M cells the trajectory does not fit perfectly. Moreover, the stimuli for the 16 dimensional and 14 dimensional model are different to the ones from Figure 3. In any case normal AP is well represented by the simplified models. In case of more complex patterns such as EADs the general dynamics of all models are identical, but to find the correct basin of attraction modifying the stimulus is more difficult.

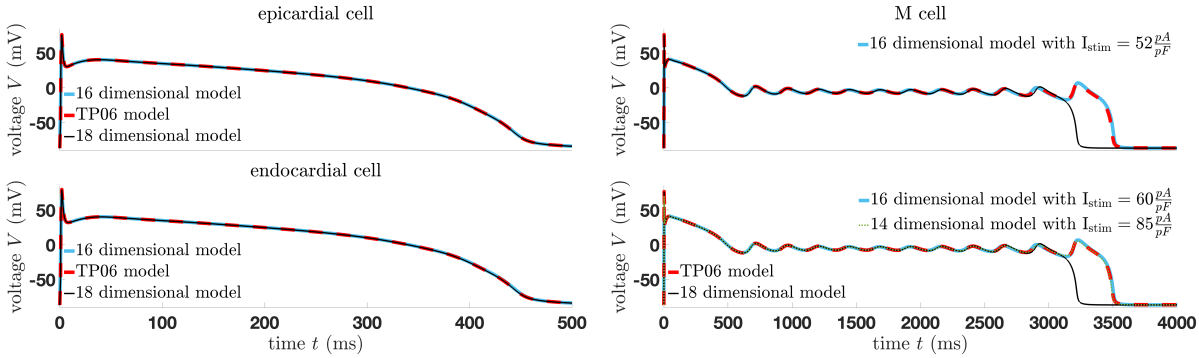

Figure 6: Comparison of the trajectories of the modified models using the standard value of $\mathrm{G_{Ks}}$ with value shifts $\mathrm{G_{Kr}} \to 0.1 \cdot \mathrm{G_{Kr}}$ and $\mathrm{G_{CaL}} \to 5 \cdot \mathrm{G_{CaL}}$.

Our next aim is to study the 14 dimensional epicardical TP06 model by means of bifurcation analysis in more detail. Our focus is on the situation as in Figure 6, i.e. we are using $\mathrm{G_{Ks}}$ as bifurcation parameter and consider a value shifts $\mathrm{G_{Kr}} \to 0.1 \cdot \mathrm{G_{Kr}}$ and $\mathrm{G_{CaL}} \to 5 \cdot \mathrm{G_{CaL}}$. This means we have a reduced rapid delayed rectifier current and an enhanced L-type calcium current. Utilizing the bifurcation analysis we can extract the behavior and the dynamics of the system. Starting a numerical continuation from a steady state solution we find two supercritical Andronov-Hopf bifurcations, cf. Table 5. From these bifurcation points a stable limit cycle branch bifurcates each. Following the limit cycle branch from the second Andronov-Hopf bifurcation ($\mathrm{G_{Ks}} \approx 0.069724\frac{nS}{pF}$) we find a torus bifurcation and a first period-doubling bifurcation. Furthermore, the limit cycle branch changes stability and finally, it will collide with the equilibrium curve and terminates there, cf. Figure 7. This behavior is similar for all investigated combinations of $(\mathrm{G_{Ks}}, \mathrm{G_{Kr}}, \mathrm{G_{CaL}})$. However, the type and position of the points vary, please compare Table 5 and Table 6. Starting a continuation from the first period-doubling bifurcation we find a second limit cycle branch containing a second period-doubling bifurcation, cf. again Figure

bifurcation points	$\mathrm{G_{Ks}}$ value	description	period
Andronov-Hopf	$\approx 0.027310 \frac{nS}{pF}$	supercritial	
	$\approx 0.069724 \frac{nS}{pF}$	supercritial	
torus	$\approx 0.072733 \frac{nS}{pF}$		≈ 259.53
period-doubling	$\approx 0.093842 \frac{nS}{pF}$	subcritial	≈ 422.67
	$\approx 0.095239 \frac{nS}{pF}$	subcritial	≈ 861.35
	$\approx 0.095572 \frac{nS}{pF}$	subcritial	≈ 1733.31

Table 5: Bifurcation for the 14 dimensional epicardial cell model with $(\mathrm{G_{Ks}}, \mathrm{G_{Kr}}, \mathrm{G_{CaL}}) \longrightarrow (\mathrm{G_{Ks}}, 0.1 \cdot \mathrm{G_{Kr}}, 5 \cdot \mathrm{G_{CaL}})$.

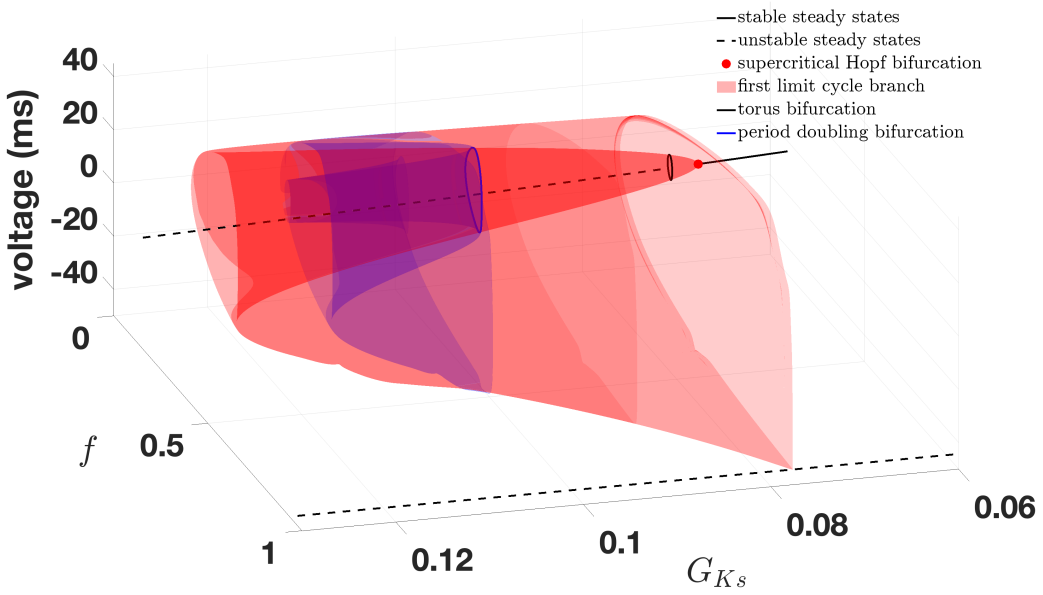

Figure 7: Bifurcation diagram of the 14 dimensional epicardial cell model with $(\mathrm{G_{Ks}}, \mathrm{G_{Kr}}, \mathrm{G_{CaL}}) \longrightarrow (\mathrm{G_{Ks}}, 0.1 \cdot \mathrm{G_{Kr}}, 5 \cdot \mathrm{G_{CaL}})$, where $\mathrm{G_{Ks}}$ is used a bifurcation parameter. The bifurcation diagram contains the second Andronov-Hopf bifurcation, the first two limit cylce branches, the torus bifurcation and the first period-doubling bifurcation.

7. Taking this approach further, it results in an unstable period-doubling cascade, cf. Figure 8, where we show a zoom on the region with the first four limit cycle branches. Based on the bifurcation diagram, we can identify a $\mathrm{G_{Ks}}$ region, where EADs may appear. This region is clearly linked to the period-doubling cascade, however, whether EADs occur or not is also dependent on the initial values and the initial stimulus. This means in case the initial values and stimulus is chosen in such a way that the trajectory is not able to enter the basin of attraction of the period-doubling cascade, then no EAD appear even though the system is in the dangerous region. This may happen for instance if the initial stimulus is high, which one may link to the usage of a pace maker.

Finally, for comparison reasons we provide the first 5 important bifurcations in the situation of the parameter shift $(\mathrm{G_{Ks}}, \mathrm{G_{Kr}}, \mathrm{G_{CaL}}) \longrightarrow (\mathrm{G_{Ks}}, 0.18 \cdot \mathrm{G_{Kr}}, 5 \cdot \mathrm{G_{CaL}})$, cf. Table 6.

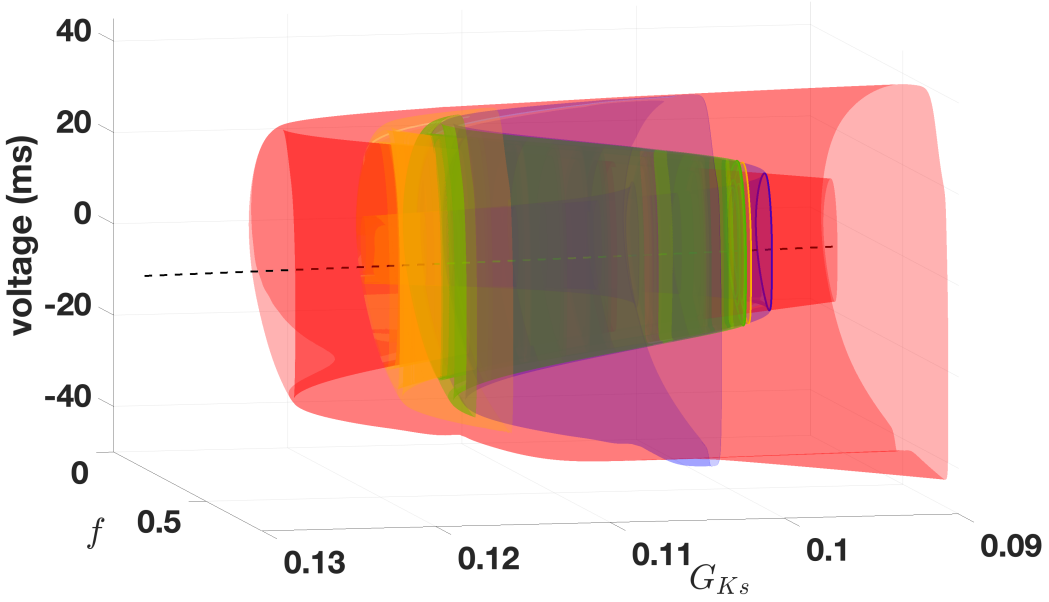

Figure 8: Zoom of Figure 7 containing the first four limit cylce branches.

bifurcation points	$\mathrm{G_{Ks}}$ value	description	period
Andronov-Hopf	$\approx 0.026278 \frac{nS}{pF}$	supercritial	
	$\approx 0.066995 \frac{nS}{pF}$	supercritial	
torus	$\approx 0.067818 \frac{nS}{pF}$		≈ 245.53
period-doubling	$\approx 0.088309 \frac{nS}{pF}$	subcritial	≈ 424.84
	$\approx 0.089585 \frac{nS}{pF}$	subcritial	≈ 865.89

Table 6: Bifurcation for the 14 dimensional epicardial cell model with $(\mathrm{G_{Ks}}, \mathrm{G_{Kr}}, \mathrm{G_{CaL}}) \longrightarrow (\mathrm{G_{Ks}}, 0.18 \cdot \mathrm{G_{Kr}}, 5 \cdot \mathrm{G_{CaL}})$.

4 Simulation of the monodomain model

The final focus of this paper, is the synchronization and pattern formation of cardiac cells. In the fashion of [71], we write the monodomain model (4) as a reaction-diffusion system, which it is, i.e.

$$\frac{\partial V}{\partial t} = D\Delta V - \frac{\mathrm{I_{ion}}(V, g) + \mathrm{I_{stim}}}{C_m}, \tag{5}$$

where D denotes the diffusion coefficient $D = \frac{\lambda}{1+\lambda} \frac{M_i}{\chi} \frac{1}{C_m}$. Moreover, we use the same mesh, time and space discretization and stimulus as in [71], see Table 7.

Spatial grid size Δx	Time step Δt	Stimulation duration	Stimulus strength	Second stimulus	Diffusion coefficient	Integration domain size
$0.25mm$	$0.05/0.02ms$	$1.5ms$	$52mV$	$340ms$	$0.154 \frac{mm^2}{ms}$	$100mm$

Table 7: Mesh, stimulation and diffusion parameters.

Notice that for normal AP simulations we use a time step of $\Delta t = 0.05ms$, while for the simulations of

EAD settings we use $\Delta t = 0.02ms$. In the following, we perform 1D and 2D simulations to investigate synchronization effects.

4.1 1D simulations

We start by considering aligned epi-, M- and endocardial cells in the left ventricle. This is motivated by the fact that the wall of the left ventricle contains three different layers [72, 73]. Therefore, we assume on the left and right side of the $100mm$ line/network a population of epi- and endocardial cells, while in between there are mid-myocardial cells. Furthermore, we assume for all cells a shift in the conductances $(\mathrm{G_{Kr}}, \mathrm{G_{CaL}}) \longrightarrow (0.1 \cdot \mathrm{G_{Kr}}, 5 \cdot \mathrm{G_{CaL}})$, which implies that the epi- and endocardial cells do not develop EADs, however, the have an elongated AP. Furthermore, the mid-myocardial cell model develops EADs. The three cell types are aligned via the one dimensional monodomain model, where all cells have the same initial condition and stimulus. Moreover, the monodomain model (5) is equipped the homogeneous Neumann boundary condition. Notice that the chosen spatial gird size implies that we consider 400 cells, where we have three situations, i.e. 392, 320 and 200 mid-myocardial cells. In Figure 9, we see how the cell network synchronizes and how the EAD, which would

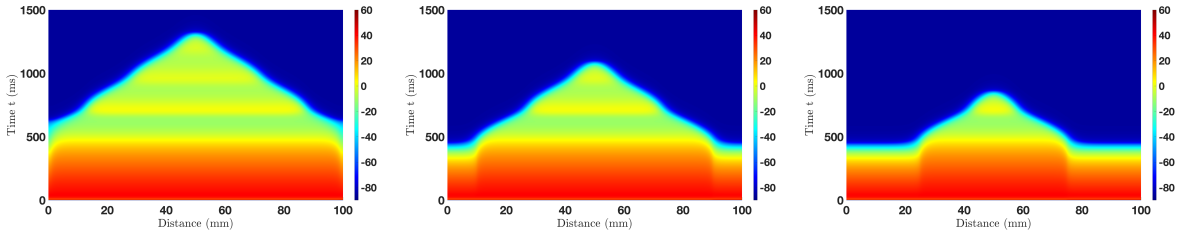

Figure 9: Comparison of the epi-, mid-myo- and endocardial cell network. (**Left**) Epi- and endocardial cells represent 2% of the population. (**Middle**) Epi- and endocardial cells represent 20% of the population. (**Right**) Epi- and endocardial cells represent 50% of the population.

last for more than $3000ms$, is compensated by the other cells, even then their population is only 2% of the whole population. This remarkable numerical experiment indicates that the heart is quite robust.

4.2 2D simulations

The simulations of the monodomain model (5) are done in FEniCS [39, 40] and the coupled ODE–PDE system is solved using cbcbeat, described in [41], and fenics-beat [42]. Again the code are provided in [46].

As in [71] we apply the S1-S2 protocol to generate spiral waves, which means we first apply to a thin strip $x \leq 10mm$ on the left side of the square region. This induces a plane wave that propagate to the right edge of the square. Then, after $340ms$ we apply a second stimulus to the lower half plane ($0 \leq x < L$ and $0 \leq y < \frac{L}{2}$, where L denotes domain size).

We restrict ourself to the epicardial human ventricular tissue model of [57] and to two different parameter settings, i.e. the normal AP setting, the parameter set $(\mathrm{G_{Ks}}, \mathrm{G_{Kr}}, \mathrm{G_{CaL}}) \longrightarrow (0.098\frac{nS}{pF}, 0.18 \cdot \mathrm{G_{Kr}}, 5 \cdot \mathrm{G_{CaL}})$. The last setting either means that we simulate the mid-myocardial model with reduced rapid delayed rectifier current and enhanced L-type calcium current or the epicardial model with reduced rapid slow and delayed rectifier current and enhanced L-type calcium current.

In Figure 10 we state for 5 different time point, where each column corresponds to one time point, (spiral wave) pattern formations. The first row presents the normal AP, while the second row the EAD setting. Here, we see that in both cases a spiral wave is initiated. In the normal AP case one has a stable spiral wave which still exists after $10000ms$, cf. Figure 11. However, in the case of EADs, we see wave break-up, where the spiral wave disappears and the AP reaches its resting potential and no further activity is recognized.

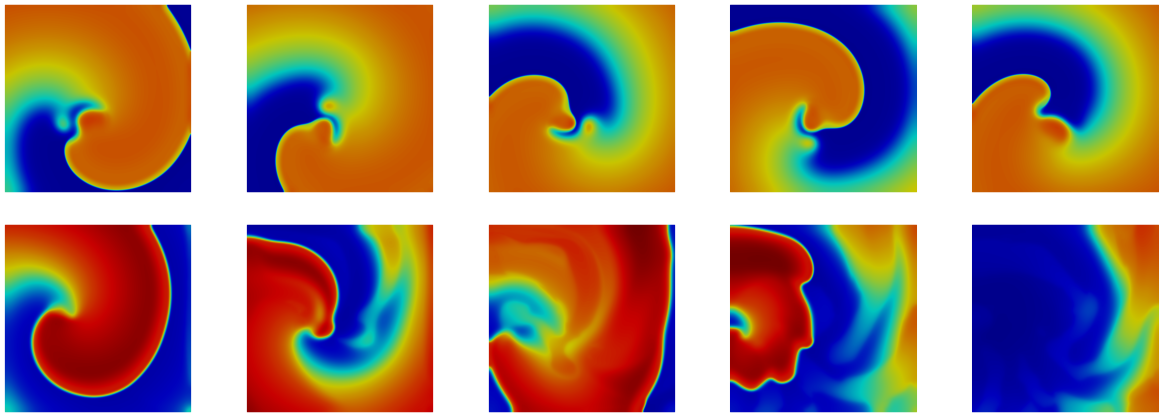

Figure 10: Comparison of spiral waves after $2000ms, 3000ms, 4000ms, 5000ms$ and $5400ms$. **(First row)** normal AP. **(Second row)** normal EAD.

This is also in line with the common knowledge that EADs can be precursors to cardiac death.

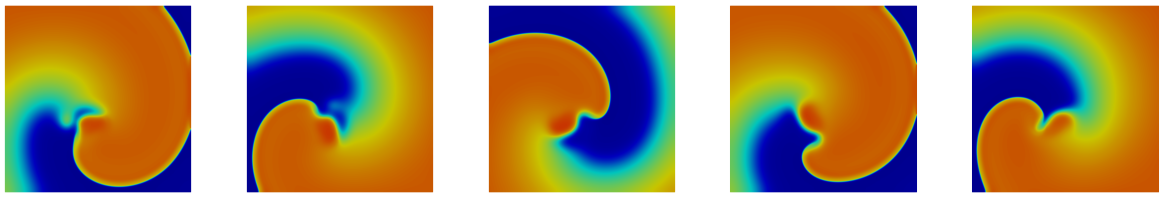

Figure 11: Spiral wave of the normal AP after $6000ms, 7000ms, 8000ms, 9000ms$ and $10000ms$.

5 Discussion

This paper is aimed to investigate the dynamics of the TP06 model [57, 56] with a focus on early afterdepolarizations. A very efficient and beneficial way to study the behavior of a dynamical system is delivered by the bifurcation theory. Thus, one main goal of the paper is the numerical bifurcation analysis of the cellular TP06 model. To this end we reported the difficulties in the modeling of the original model, which is also highlighted in [35, 36]. In addition, we discussed several possible modifications and model reductions of the TP06 model which allow to perform numerical bifurcation analysis and to apply the numerical continuation algorithm provided in [44, 45]. Thus, we are able to reduce the 19 dimensional TP06 model up to an 14 dimensional version, which has (almost) identical dynamics and trajectories as the original model, cf. Figure 5 and Tables 2, 3 and 4. This model reduction allows not only to perform numerical bifurcation, it also decreases the numerical effort and time. Apart from the steady state dynamics which are (almost) identically, one has to adjusts the initial stimulus such that

the trajectory is able to enter the same basin of attraction. Moreover, in Figure 6 it is illustrated that finding the correct basin of attraction is more difficult for complex dynamics and pattern.

After the remodeling, using the set of parameters $(\mathrm{G_{Ks}}, \mathrm{G_{Kr}}, \mathrm{G_{CaL}})$, which are known to induce EADs for certain combinations of values, cf. e.g. [8, 7], a systematical bifurcation analysis is provided. The (numerical) bifurcation analysis shows that the oscillatory behavior of the TP06 model and its modified versions is induced by a Andronov-Hopf bifurcation and the occurrence of EADs is related to the existence of an unstable period-doubling bifurcation cascade. Moreover, deterministic chaos is not observed which is in line with [47, 36, 74]. We show that even though the system is in a dangerous reason and EADs potentially occur, the initial values and initial stimulus decides whether the trajectory enters the basin of attraction of the period-doubling bifurcation cascade. Therefore, we have three driving forces that induce EADs, the steady state dynamics of the system, the initial values and the initial stimulus. This knowledge can now used to prevent the occurrence of EADs.

Furthermore, the performed numerical experiments how networks of cells in 1D and 2D synchronize. Here, we can extract from our investigation on one hand how robust a cell network reacts on EADs, cf. Figure 9, on the other hand see can see how stable pattern appears, see Figure 10 (first row) and Figure 11. In addition, we showed that EADs may induce a wave break-up, see Figure 10 (second row).

In summary, this study provides an approach and codes to efficient investigate cardiac dynamics numerically. We showed on tissue level that the local steady state dynamics of the system incudes certain pattern formation. Furthermore, we found that also the diffusivity of the system, the initial configuration and the initial stimulus is highly important for the pattern formation and the network dynamics. This has to be studied in more detail and is part of a future study.

Conflict of Interest Statement

The author declares no conflict of interest.

References

[1] K. Tsaneva-Atanasova and V. Diaz-Zuccarini, “Editorial: Mathematics for healthcare as part of computational medicine,” *Frontiers in Physiology*, vol. 9, 2018.

[2] L. Xia, H. Zhang, and D. Zheng, “Editorial: Multi-scale computational cardiology,” *Frontiers in Physiology*, vol. 13, 2022.

[3] A. H. Erhardt, K. Tsaneva-Atanasova, G. T. Lines, and E. A. Martens, “Editorial: Dynamical systems, pdes and networks for biomedical applications: Mathematical modeling, analysis and simulations,” *Frontiers in Physics*, vol. 10, 2023.

[4] A. H. Erhardt, D. Peschka, C. Dazzi, L. Schmeller, A. Petersen, S. Checa, A. Münch, and B. Wagner, “Modeling cellular self-organization in strain-stiffening hydrogels,” *Computational Mechanics*, vol. to appear, 2024.

[5] E. M. Cherry, F. H. Fenton, T. Krogh-Madsen, S. Luther, and U. Parlitz, “Introduction to focus issue: Complex cardiac dynamics,” *Chaos: An Interdisciplinary Journal of Nonlinear Science*, vol. 27, no. 9, p. 093701, 2017.

[6] A. H. Erhardt, K. Tsaneva-Atanasova, G. T. Lines, and E. A. Martens, eds., *Dynamical Systems, PDEs and Networks for Biomedical Applications: Mathematical Modeling, Analysis and Simulations*. Lausanne: Frontiers Media SA, 2023.

[7] E. Van Nieuwenhuyse, G. Seemann, A. V. Panfilov, and N. Vandersickel, "Effects of early afterdepolarizations on excitation patterns in an accurate model of the human ventricles," *PLOS ONE*, vol. 12, pp. 1–19, 12 2017.

[8] S. Zimik, N. Vandersickel, A. R. Nayak, A. V. Panfilov, and R. Pandit, "A comparative study of early afterdepolarization-mediated fibrillation in two mathematical models for human ventricular cells," *PLOS ONE*, vol. 10, pp. 1–20, 06 2015.

[9] A. Tveito, K.-A. Mardal, and M. E. Rognes, eds., *Modeling Excitable Tissue*. Springer, 2021.

[10] K.-A. Mardal, M. E. Rognes, T. B. Thompson, and L. M. Valnes, eds., *Mathematical Modeling of the Human Brain*. Springer, 2022.

[11] S. A. Niederer, J. Lumens, and N. A. Trayanova, "Computational models in cardiology," *Nature reviews cardiology*, vol. 16, no. 2, pp. 100–111, 2019.

[12] F. B. Sachse, *Computational cardiology: modeling of anatomy, electrophysiology, and mechanics*, vol. 2966. Springer Science & Business Media, 2004.

[13] A. Bueno-Orovio, E. M. Cherry, and F. H. Fenton, "Minimal model for human ventricular action potentials in tissue," *Journal of Theoretical Biology*, vol. 253, no. 3, pp. 544–560, 2008.

[14] R. Clayton, O. Bernus, E. Cherry, H. Dierckx, F. Fenton, L. Mirabella, A. Panfilov, F. Sachse, G. Seemann, and H. Zhang, "Models of cardiac tissue electrophysiology: Progress, challenges and open questions," *Progress in Biophysics and Molecular Biology*, vol. 104, no. 1, pp. 22–48, 2011. Cardiac Physiome project: Mathematical and Modelling Foundations.

[15] Y. A. Kuznetsov, *Elements of Applied Bifurcation Theory*. Springer-Verlag, New York, 2004.

[16] N. Fenichel, "Geometric singular perturbation theory for ordinary differential equations," *J. Differ. Equ.*, vol. 31, no. 1, pp. 53 – 98, 1979.

[17] K. Tsumoto, T. Shimamoto, Y. Aoji, Y. Himeno, Y. Kuda, M. Tanida, A. Amano, and Y. Kurata, "Theoretical prediction of early afterdepolarization-evoked triggered activity formation initiating ventricular reentrant arrhythmias," *Computer Methods and Programs in Biomedicine*, vol. 240, p. 107722, 2023.

[18] R. Barrio, J. Jover-Galtier, M. Martínez, L. Pérez, and S. Serrano, "Mathematical birth of early afterdepolarizations in a cardiomyocyte model," *Mathematical Biosciences*, vol. 366, p. 109088, 2023.

[19] K. Tsumoto and Y. Kurata, "Bifurcations and proarrhythmic behaviors in cardiac electrical excitations," *Biomolecules*, vol. 12, no. 3, 2022.

[20] Y. Kurata, K. Tsumoto, K. Hayashi, I. Hisatome, Y. Kuda, and M. Tanida, "Multiple dynamical mechanisms of phase-2 early afterdepolarizations in a human ventricular myocyte model: Involvement of spontaneous sr ca2+release," *Frontiers in Physiology*, vol. 10, 2020.

[21] H. Kitajima and T. Yazawa, "Bifurcation analysis on a generation of early afterdepolarization in a mathematical cardiac model," *International Journal of Bifurcation and Chaos*, vol. 31, no. 12, p. 2150179, 2021.

[22] K. Tsumoto, Y. Kurata, K. Furutani, and Y. Kurachi, "Hysteretic dynamics of multi-stable early afterdepolarisations with repolarisation reserve attenuation: A potential dynamical mechanism for cardiac arrhythmias," *Scientific Reports*, vol. 7, no. 1, p. 10771, 2017.

[23] J. Kimrey, T. Vo, and R. Bertram, "Big ducks in the heart: Canard analysis can explain large early afterdepolarizations in cardiomyocytes," *SIAM Journal on Applied Dynamical Systems*, vol. 19, no. 3, pp. 1701–1735, 2020.

[24] R. Barrio, M. A. Martínez, E. Pueyo, and S. Serrano, "Dynamical analysis of early afterdepolarization patterns in a biophysically detailed cardiac model," *Chaos: An Interdisciplinary Journal of Nonlinear Science*, vol. 31, no. 7, p. 073137, 2021.

[25] C. O. Diekman and N. Wei, "Circadian rhythms of early afterdepolarizations and ventricular arrhythmias in a cardiomyocyte model," *Biophysical Journal*, vol. 120, no. 2, pp. 319–333, 2021.

[26] R. Barrio, M. A. Martínez, S. Serrano, and E. Pueyo, "Dynamical mechanism for generation of arrhythmogenic early afterdepolarizations in cardiac myocytes: Insights from in silico electrophysiological models," *Phys. Rev. E*, vol. 106, p. 024402, Aug 2022.

[27] A. H. Erhardt, "Early afterdepolarisations induced by an enhancement in the calcium current," *Processes*, vol. 7, no. 1, 2019.

[28] S. Otte, S. Berg, S. Luther, and U. Parlitz, "Bifurcations, chaos, and sensitivity to parameter variations in the sato cardiac cell model," *Communications in Nonlinear Science and Numerical Simulation*, vol. 37, pp. 265–281, 2016.

[29] A. Loppini, A. Gizzi, C. Cherubini, E. M. Cherry, F. H. Fenton, and S. Filippi, "Spatiotemporal correlation uncovers characteristic lengths in cardiac tissue," *Phys. Rev. E*, vol. 100, p. 020201, Aug 2019.

[30] M. Peirlinck, F. Costabal, J. Yao, and et al., "Precision medicine in human heart modeling," *Biomech. Model. Mechanobiol.*, vol. 20, 2021.

[31] N. A. Trayanova and P. M. Boyle, "Advances in modeling ventricular arrhythmias: from mechanisms to the clinic," *WIREs Systems Biology and Medicine*, vol. 6, no. 2, pp. 209–224, 2014.

[32] N. A. Trayanova, A. N. Doshi, and A. Prakosa, "How personalized heart modeling can help treatment of lethal arrhythmias: A focus on ventricular tachycardia ablation strategies in post-infarction patients," *WIREs Systems Biology and Medicine*, vol. 12, no. 3, p. e1477, 2020.

[33] A. Dasí, A. Roy, R. Sachetto, J. Camps, A. Bueno-Orovio, and B. Rodriguez, "In-silico drug trials for precision medicine in atrial fibrillation: From ionic mechanisms to electrocardiogram-based predictions in structurally-healthy human atria," *Frontiers in Physiology*, vol. 13, 2022.

[34] N. A. Trayanova, A. Lyon, J. Shade, and J. Heijman, "Computational modeling of cardiac electrophysiology and arrhythmogenesis: toward clinical translation," *Physiological Reviews*, vol. 104, no. 3, p. 1265, 2023.

[35] P. Rose, J.-H. Schleimer, and S. Schreiber, "Modifications of sodium channel voltage dependence induce arrhythmia-favouring dynamics of cardiac action potentials," *PLOS ONE*, vol. 15, pp. 1–14, 08 2020.

[36] A. H. Erhardt and S. Solem, "Bifurcation analysis of a modified cardiac cell model," *SIAM Journal on Applied Dynamical Systems*, vol. 21, no. 1, pp. 231–247, 2022.

[37] C. H. Luo and Y. Rudy, "A model of the ventricular cardiac action potential. depolarization, repolarization, and their interaction.," *Circulation Research*, vol. 68, no. 6, pp. 1501–1526, 1991.

[38] O. Bernus, R. Wilders, C. W. Zemlin, H. Verschelde, and A. V. Panfilov, "A computationally efficient electrophysiological model of human ventricular cells," *American Journal of Physiology-Heart and Circulatory Physiology*, vol. 282, no. 6, pp. H2296–H2308, 2002.

[39] M. S. Alnaes, J. Blechta, J. Hake, A. Johansson, B. Kehlet, A. Logg, C. Richardson, J. Ring, M. E. Rognes, and G. N. Wells, "The FEniCS project version 1.5," *Archive of Numerical Software*, vol. 3, 2015.

[40] A. Logg, K. Mardal, and G. N. Wells, *Automated Solution of Differential Equations by the Finite Element Method*. Springer, 2012.

[41] M. E Rognes, P. E Farrell, S. W Funke, J. E Hake, and M. MC Maleckar, "cbcbeat: an adjoint-enabled framework for computational cardiac electrophysiology," *The Journal of Open Source Software*, vol. 2, 2017.

[42] H. Finsberg, "fenics-beat," *Github*, Aug. 2024.

[43] S. Rush and H. Larsen, "A practical algorithm for solving dynamic membrane equations," *IEEE Transactions on Biomedical Engineering*, vol. BME-25, no. 4, pp. 389–392, 1978.

[44] A. Dhooge, W. Govaerts, and Y. A. Kuznetsov, "Matcont: A matlab package for numerical bifurcation analysis of odes," *ACM Trans. Math. Softw.*, vol. 29, pp. 141–164, June 2003.

[45] A. Dhooge, W. Govaerts, Y. A. Kuznetsov, H. G. E. Meijer, and B. Sautois, "New features of the software matcont for bifurcation analysis of dynamical systems," *Math. Comput. Model. Dyn. Syst.*, vol. 14, no. 2, pp. 147–175, 2008.

[46] A. H. Erhardt, *Cardiac dynamics of a human ventricular tissue model with focus on early afterdepolarizations*, 2024. https://github.com/andreerhardt/cardiac-dynamics-of-a-human-ventricular-tissue-model-with-focus-on-ea

[47] A. H. Erhardt and S. Solem, "On complex dynamics in a purkinje and a ventricular cardiac cell model," *Communications in Nonlinear Science and Numerical Simulation*, vol. 93, p. 105511, 2021.

[48] Z. Qu, "Chaos in the genesis and maintenance of cardiac arrhythmias," *Progress in Biophysics and Molecular Biology*, vol. 105, no. 3, pp. 247–257, 2011. Muscle Excitation-Contraction Coupling: Elements and Integration.

[49] M. Dix, T. Lilienkamp, S. Luther, and U. Parlitz, "Influence of conduction heterogeneities on transient spatiotemporal chaos in cardiac excitable media," *Phys. Rev. E*, vol. 110, p. 044207, Oct 2024.

[50] D. Suth, S. Luther, and T. Lilienkamp, “Chaos control in cardiac dynamics: terminating chaotic states with local minima pacing,” *Frontiers in Network Physiology*, vol. 4, 2024.

[51] K. H. Jæger, V. Charwat, B. Charrez, H. Finsberg, M. M. Maleckar, S. Wall, K. E. Healy, and A. Tveito, “Improved computational identification of drug response using optical measurements of human stem cell derived cardiomyocytes in microphysiological systems,” *Frontiers in Pharmacology*, vol. 10, 2020.

[52] A. Tveito, M. M. Maleckar, and G. T. Lines, “Computing optimal properties of drugs using mathematical models of single channel dynamics,” *Computational and Mathematical Biophysics*, vol. 6, no. 1, pp. 41–64, 2018.

[53] X. Zhou, Y. Qu, E. Passini, A. Bueno-Orovio, Y. Liu, H. M. Vargas, and B. Rodriguez, “Blinded in silico drug trial reveals the minimum set of ion channels for torsades de pointes risk assessment,” *Frontiers in Pharmacology*, vol. 10, 2020.

[54] F. Margara, Z. J. Wang, F. Levrero-Florencio, A. Santiago, M. Vázquez, A. Bueno-Orovio, and B. Rodriguez, “In-silico human electro-mechanical ventricular modelling and simulation for drug-induced pro-arrhythmia and inotropic risk assessment,” *Progress in Biophysics and Molecular Biology*, vol. 159, pp. 58–74, 2021. Mechanobiology of the Cardiovascular System.

[55] E. Passini, X. Zhou, C. Trovato, O. J. Britton, A. Bueno-Orovio, and B. Rodriguez, “The virtual assay software for human in silico drug trials to augment drug cardiac testing,” *Journal of Computational Science*, vol. 52, p. 101202, 2021. Case Studies in Translational Computer Science.

[56] K. H. W. J. ten Tusscher, D. Noble, P. J. Noble, and A. V. Panfilov, “A model for human ventricular tissue,” *American Journal of Physiology-Heart and Circulatory Physiology*, vol. 286, no. 4, pp. H1573–H1589, 2004. PMID: 14656705.

[57] K. H. W. J. ten Tusscher and A. V. Panfilov, “Alternans and spiral breakup in a human ventricular tissue model,” *American Journal of Physiology-Heart and Circulatory Physiology*, vol. 291, no. 3, pp. H1088–H1100, 2006. PMID: 16565318.

[58] A. L. Hodgkin and A. F. Huxley, “A quantitative description of membrane current and its application to conduction and excitation in nerve,” *J. Physiol.*, vol. 117, no. 4, pp. 500–544, 1952.

[59] T. J. Hund, J. P. Kucera, N. F. Otani, and Y. Rudy, “Ionic charge conservation and long-term steady state in the luo–rudy dynamic cell model,” *Biophysical Journal*, vol. 81, no. 6, pp. 3324–3331, 2001.

[60] K. H. W. J. T. Tusscher and A. V. Panfilov, “Cell model for efficient simulation of wave propagation in human ventricular tissue under normal and pathological conditions,” *Physics in Medicine & Biology*, vol. 51, p. 6141, nov 2006.

[61] A. Tveito, K. H. Jæger, M. Kuchta, K.-A. Mardal, and M. E. Rognes, “A cell-based framework for numerical modeling of electrical conduction in cardiac tissue,” *Frontiers in Physics*, vol. 5, 2017.

[62] K. H. Jæger, K. G. Hustad, X. Cai, and A. Tveito, “Efficient numerical solution of the emi model representing the extracellular space (e), cell membrane (m) and intracellular space (i) of a collection of cardiac cells,” *Frontiers in Physics*, vol. 8, 2021.

[63] A. J. Ellingsrud, A. Solbrå, G. T. Einevoll, G. Halnes, and M. E. Rognes, “Finite element simulation of ionic electrodiffusion in cellular geometries,” *Frontiers in Neuroinformatics*, vol. 14, 2020.

[64] P. Benedusi, A. J. Ellingsrud, H. Herlyng, and M. E. Rognes, "Scalable approximation and solvers for ionic electrodiffusion in cellular geometries," *SIAM Journal on Scientific Computing*, vol. 46, no. 5, pp. B725–B751, 2024.

[65] M. K. Mulimani, S. Zimik, and R. Pandit, "An in silico study of electrophysiological parameters that affect the spiral-wave frequency in mathematical models for cardiac tissue," *Frontiers in Physics*, vol. 9, 2022.

[66] B. A. Lawson, R. W. dos Santos, I. W. Turner, A. Bueno-Orovio, P. Burrage, and K. Burrage, "Homogenisation for the monodomain model in the presence of microscopic fibrotic structures," *Communications in Nonlinear Science and Numerical Simulation*, vol. 116, p. 106794, 2023.

[67] S. Alonso, M. Bär, and B. Echebarria, "Nonlinear physics of electrical wave propagation in the heart: a review," *Reports on Progress in Physics*, vol. 79, p. 096601, aug 2016.

[68] K. H. Jæger and A. Tveito, "Deriving the bidomain model of cardiac electrophysiology from a cell-based model; properties and comparisons," *Frontiers in Physiology*, vol. 12, 2022.

[69] J. Sundnes, G. Lines, B. Nielsen, K.-A. Mardal, and A. Tveito, eds., *Computing the electrical activity in the heart*. Springer, 2006.

[70] A. H. Erhardt, "Bifurcation analysis of a certain Hodgkin–Huxley model depending on multiple bifurcation parameters," *Mathematics*, vol. 6, no. 6, pp. 1–15, 2018.

[71] S. F. Pravdin, T. I. Epanchintsev, and A. V. Panfilov, "Overdrive pacing of spiral waves in a model of human ventricular tissue," *Scientific Reports*, vol. 10, no. 1, p. 20632, 2020.

[72] M. Litvinuková, C. Talavera-López, H. Maatz, and et al., "Cells of the adult human heart," *Nature*, p. 466–472, 2020.

[73] R. H. Clayton and A. V. Holden, "Propagation of normal beats and re-entry in a computational model of ventricular cardiac tissue with regional differences in action potential shape and duration," *Progress in Biophysics and Molecular Biology*, vol. 85, no. 2, pp. 473–499, 2004. Modelling Cellular and Tissue Function.

[74] P. Kügler, M. Bulelzai, and A. Erhardt, "Period doubling cascades of limit cycles in cardiac action potential models as precursors to chaotic early afterdepolarizations," *BMC Syst Biol*, vol. 11, 2017.